Molecular Electronics

International Edition: DOI: 10.1002/anie.201904521
German Edition: DOI: 10.1002/ange.201904521

Multicenter-Bond-Based Quantum Interference in Charge Transport Through Single-Molecule Carborane Junctions

Chun Tang, Lijue Chen, Longyi Zhang, Zhixin Chen, Guopeng Li, Zhewei Yan, Luchun Lin, Junyang Liu, Longfeng Huang, Yiling Ye, Yuhui Hua, Jia Shi, Haiping Xia, and Wenjing Hong**

Abstract: *Molecular components are vital to introduce and manipulate quantum interference (QI) in charge transport through molecular electronic devices. Up to now, the functional molecular units that show QI are mostly found in conventional π- and σ-bond-based systems; it is thus intriguing to study QI in multicenter bonding systems without both π- and σ-conjugations. Now the presence of QI in multicenter-bond-based systems is demonstrated for the first time, through the single-molecule conductance investigation of carborane junctions. We find that all the three connectivities in carborane frameworks show different levels of destructive QI, which leads to highly suppressed single-molecule conductance in para- and meta-connected carboranes. The investigation of QI into carboranes provides a promising platform to fabricate molecular electronic devices based on multicenter bonds.*

Quantum interference (QI) offers the unique opportunity to tune charge transport through molecular devices and materials,[1] which leads to various applications such as QI-based thermoelectrics,[2] molecular memory,[3] molecular transistors,[4] and sensors.[5] The molecular building blocks play a vital role in investigating QI-based molecular junctions. Up to now, the molecular building blocks with QI are mostly found in conventional two-center–two-electron (2c–2e) bond-based systems, which lead to π-interference[1d,3,4,6] and σ-interference.[2b] In the π systems, the involvement of σ bonds are inevitable, and the π-interference can only suppress the π channels, leaving the σ channels unaffected. When the molecular building blocks are only constructed from σ bonds with the vanishing of π channels, the σ-interference will lead to strong conductance suppression, as recently demonstrated in σ-conjugated silane system.[2b] Besides the 2c–2e bond-based system, inorganic clusters based on metal–metal bonds were also found to show QI.[7] These progresses suggest the great potential of exploring QI in distinctive bonding systems.

Besides the conventional 2c–2e bonds, there exist abundantly unconventional multicenter bonding systems, showing much richer patterns to form bonds with the absence of both π and σ conjugations (Figure 1a). Thus, whether and how QI is present in those multicenter bonding systems become an unexplored and promising avenue. To explore such multicenter-bond-based QI, carborane is an ideal molecular building block. Since the carborane framework is constructed from three-center–two-electron (3c–2e) bonds, the electrons of the 3c–2e bonds can delocalize around the framework, ensuring efficient conjugation between each multicenter bond. The efficient conjugation of carborane leads to distinctively three-dimensional aromaticity[8] and high stability,[9] which has already been applied in a broad spectrum of fields,[9b,10] such as catalysis,[11] supramolecular chemistry,[12] and optoelectronics.[13] Thus the single-molecule conductance investigation of carborane provides an ideal testbed to investigate the multicenter-bond-based QI, which will be a benchmark for multicenter bonds based molecular electronic devices.

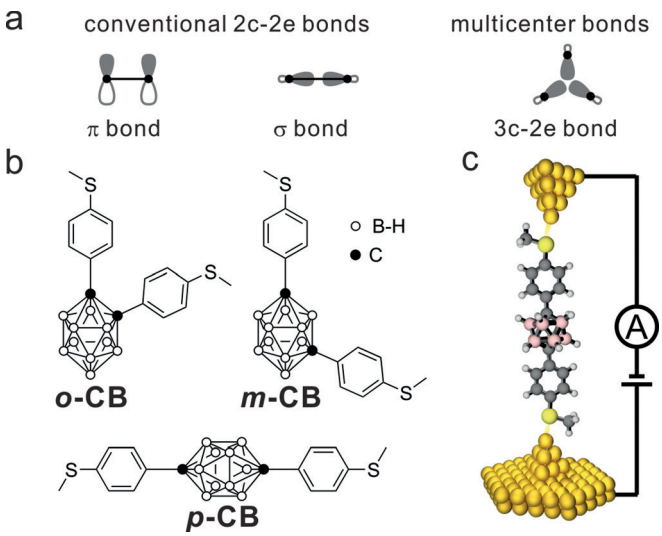

Figure 1. a) Example of conventional bonds and multicenter bonds. b) The molecular structures of carboranes with three different connectivities. The white cycles represent the B−H group, and the solid black cycles represent carbon atoms. c) The STM-BJ setup for measuring the single-molecule conductance of carboranes.

Herein, we demonstrate the existence of QI in the unique multicenter bonding system for the first time, through the single-molecule conductance investigation of the carborane system using the scanning tunneling microscope break junction (STM-BJ) technique (Figure 1c). We find that all

[*] C. Tang, L. Chen, L. Zhang, Dr. Z. Chen, G. Li, Z. Yan, Dr. L. Lin, Dr. J. Liu, L. Huang, Y. Ye, Y. Hua, Dr. J. Shi, Prof. Dr. H. Xia, Prof. Dr. W. Hong
State Key Laboratory of Physical Chemistry of Solid Surfaces, College of Chemistry and Chemical Engineering, Collaborative Innovation Centre of Chemistry for Energy Materials (*i*ChEM), Xiamen University
Xiamen 361005 (China)
E-mail: hpxia@xmu.edu.cn
whong@xmu.edu.cn
Supporting information and the ORCID identification number(s) for the author(s) of this article can be found under: https://doi.org/10.1002/anie.201904521.

the three connectivities in the carborane framework show different degrees of destructive QI (Figure 1b), leading to highly suppressed single-molecule conductances in *meta*-connected carboranes, while the conductance suppression of destructive QI in *ortho*-connected carboranes is alleviated through an intramolecular though-space pathway.

To fabricate the carborane-based single-molecule junctions, as shown in Figure 1b, we synthesized ***o*-CB**, ***m*-CB**, and ***p*-CB** by attaching thioanisoles as anchor groups to the two carbons of carboranes (see the Supporting Information for more details). From the lattice structures of the three molecules (Supporting Information, Figures S16–S18), we found that the intermolecular interactions are weak, which would facilitate the formation of single-molecule junctions. The crystal structures give the detailed bonding geometries of the investigated molecules (Supporting Information Figure S19). We found that the C–C bond in ***o*-CB** is 1.74 Å, which is significantly longer than the conventional C–C single bonds (1.50–1.55 Å). Meanwhile, the C–B and B–B bonds in the carborane cages show similar bond lengths to the C–C bond in the carborane cage of ***o*-CB**, which is the character of efficient delocalization in the carborane cage, with the involvement of unconventional 3c–2e bonds.

The single-molecule conductances are characterized using the STM-BJ technique in 1,2,4-trichlorobenzene with 0.25 mM target molecules at room temperature, with 100 mV bias applied between the gold tip and substrate. Typical conductance–displacement traces are shown in the inset of Figure 2a with distinct conductance plateaus at different conductance ranges. For statistical analysis, the one-dimensional (1D) histograms are constructed from 5000 individual conductance–distance traces without data selection (Figure 2a). A sharp peak around G_0 indicates the formation of Au–Au atomic point contacts,[14] and clear conductance plateaus are observed as shown in the inset of Figure 2a. The most probable conductance values determined from Gaussian fitting are $10^{-2.93\pm0.42}\,G_0$ for ***o*-CB**, $10^{-4.58\pm0.46}\,G_0$ for ***p*-CB**, and $10^{-5.14\pm0.63}\,G_0$ for ***m*-CB**. Since the junction formation probability for the three connectivities of carborane is high (Supporting Information, Figure S8), it is likely that more than one molecule could be wired parallel within the molecular junctions, which would not significantly alter the relative difference of their molecular conductances. There is also a shoulder peak centered around $10^{-3.0}\,G_0$ in the conductance histogram of ***m*-CB**. To reveal the nature of this shoulder peak, we performed the control experiment to measure the single-molecule conductance of carborane with only one thioanisole anchor (Supporting Information, Figure S11). We also observed the formation of a molecular junction, with a molecule peak centered at $10^{-3.01\pm0.49}\,G_0$, suggesting the shoulder peak of ***m*-CB** could be attributed to the formation of molecular junctions between the carborane cages and one of the two methylthio anchors, critically, we think such interaction from carborane cage is more likely to result from one of its B–H bonds.[15]

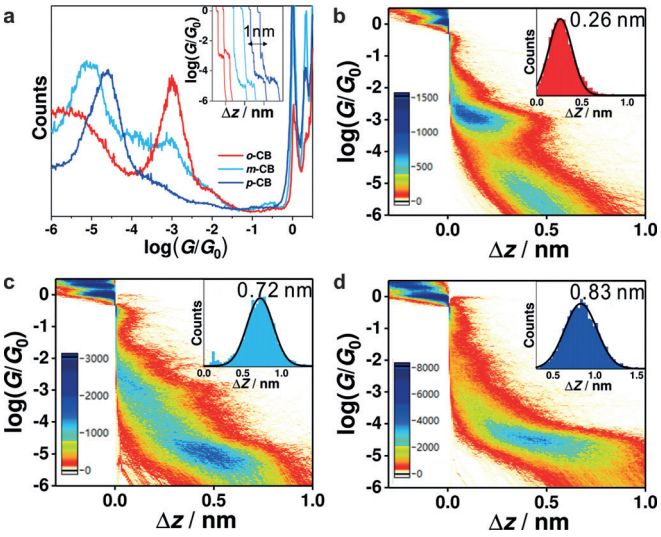

Figure 2. a) All data-point one-dimensional conductance histograms constructed from the STM-BJ traces of ***o*-CB**, ***m*-CB**, and ***p*-CB**, with their typical individual traces shown in the inset. b)–d) Two-dimensional conductance histograms of b) ***o*-CB**, c) ***m*-CB**, and d) ***p*-CB** with stretching distance Δz distributions shown in the inset; peak centers are labeled by Gaussian fitting.

To further understand the conductance difference, we analyzed the two-dimensional (2D) conductance–displacement histogram. As shown in Figure 2b, ***o*-CB** shows a conductance cloud around $10^{-3.0}\,G_0$ with 0.43 nm relative stretching displacement (inset in Figure 2b). After calibration by adding 0.50 nm snap-back distance of gold electrodes,[16] the actual junction length for the ***o*-CB** is about 0.93 nm. In comparison with ***o*-CB**, the 2D conductance–displacement histograms of ***m*-CB** and ***p*-CB** show longer stretching distances, with circa 1.22 nm and circa 1.33 nm junction lengths for ***m*-CB** (Figure 2c) and ***p*-CB** (Figure 2d), respectively. The stretching distances are consistent with the S–S distances in the crystal structures (Supporting Information, Figure S19),[17] suggesting that the formation of carborane junctions is via the two –SMe anchors. Although the conductances of molecular wires attenuate with the increase of junction lengths,[1a,18] the longer junction of ***p*-CB** still shows higher conductance than ***m*-CB**, indicating that the connectivity of electrodes into the carborane framework plays a vital role to tune the charge transport through single-molecule carborane junctions. It is intriguing that the single-molecule-scale characterization of the conductivity of carboranes is also correlated to the conductivity of carborane-based conducting polymers, in which the polymer films constructed from *ortho*-connected carborane monomer shows higher conductivity than that based on *meta*- and *para*-connected carborane monomers.[19] A similar trend was also observed in the phosphorescent organic light-emitting diodes in that the *meta*- and *para*-connected carboranes act as an insulated spacer, while the charge transfer through *ortho*-connected carborane is much more efficient.[13] The conductance of ***m*-CB** is even lower than the reported molecules with destructive QI within the length of 1.2 nm, such as the silane system with σ-interference.[2b]

To reveal the charge transport pathway through the three different carborane junctions, we further performed flicker noise analysis on their conductance plateaus. During the flicker noise measurement, junction elongation was paused

for 150 ms at the conductance range where the molecular junctions are likely to form (the typical traces are shown in Figure 3a), and the conductance plateaus within the period were extracted for noise analysis (details of flicker noise analysis are shown in Section 4 of the Supporting Information).

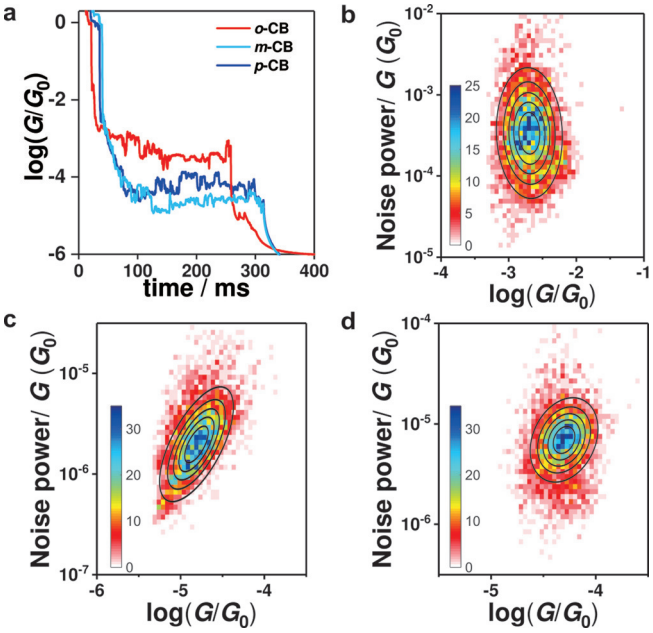

Figure 3. a) Typical traces for the noise measurement. b–d) Two-dimensional histogram of normalized flicker noise power versus average conductance for b) ***o*-CB**, c) ***m*-CB** and d) ***p*-CB**.

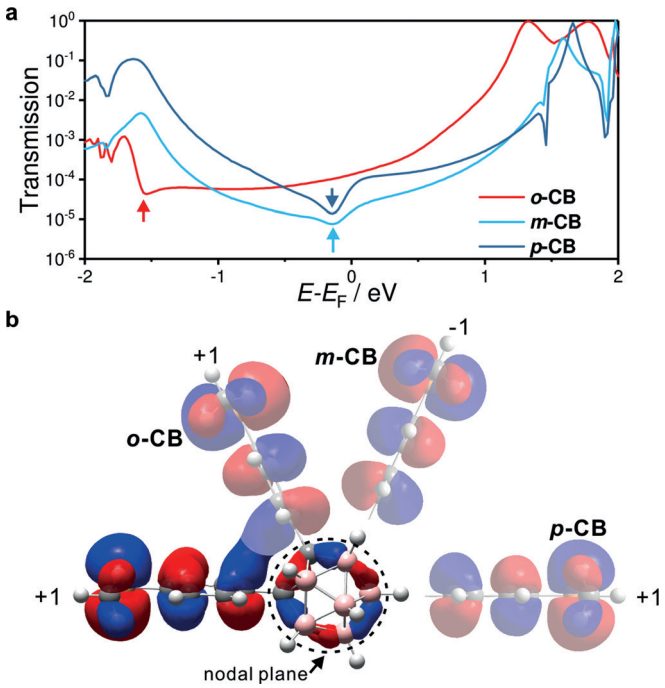

Figure 4. a) The calculated transmission coefficients of the molecule ***o*-CB**, ***m*-CB**, and ***p*-CB** versus $E-E_F$ [eV]. The arrows represent the features of destructive quantum interference. b) The orbital isosurface of the HOMO of ***o*-CB**, with 0.015 isovalue. The dashed line represents the nodal plane. Moving the semitransparent phenyl group of ***o*-CB** to the *meta*- or *para*-connectivity of carborane frameworks, forms the resemblance HOMO of ***m*-CB** or ***p*-CB** respectively. The signs of the orbital coefficients of the sulfur atoms are shown beside.

tion). According to previous results,[2b,20] the noise power of through-space coupling scales as $G^{2.0}$ (G is the mean conductance); in contrast, the noise power of the through-bond coupling scales as $G^{1.0}$. As shown in Figure 3b, we found that the noise power of ***o*-CB** scales as $G^{1.0}$, suggesting that through-bond coupling dominates the charge transport through ***o*-CB**. The noise power of ***p*-CB** (Figure 3d) scales as $G^{1.3}$, suggesting the presence of partially through-space coupling. The through-space coupling becomes dominant in *meta*-connected ***m*-CB** with its noise power scaling as $G^{1.9}$ (Figure 3c). The flicker noise analysis of the three carborane junctions reveals that the higher conductance of ***o*-CB** is associated with stronger through-bond coupling, which becomes weaker in ***m*-CB** and ***p*-CB**. The connectivity-dependent coupling between molecules and electrodes further suggests that QI may appear in the charge transport through single-molecule carborane junctions (see more details in Section 4 of the Supporting Information).[20,21]

To confirm the presence of QI, we carried out density functional theory (DFT) calculations to get the zero-bias transmission spectra of all the three molecules using the ATK software package with non-equilibrium Green's functions (NEGF).[22] As shown in Figure 4a, we find that ***p*-CB** shows higher transmission probability than ***m*-CB** in almost all the energy choice, which agrees well with the conductance trend in the experiment. In the calculated transmission functions, the HOMO–LUMO gaps of all the three connectivities are quite similar with circa 3 eV energy difference, indicating that the variation of single-molecule conductance is not from the difference of the HOMO–LUMO gaps. More interestingly, we find that all the three connectivities of carborane framework show anti-resonance transmission (as marked with arrows in Figure 4a), which indicates that the destructive QI exists in all the three connectivities, even for the *para*-connectivity, which typically shows constructive QI in π-conjugated molecules. For ***o*-CB**, the occurrence of anti-resonance transmission is far away from the Fermi energy, which is in contrast to the anti-resonance transmissions of ***p*-CB** and ***m*-CB** closing to the Fermi energy. These results reveal that the high conductance of ***o*-CB** in the experiment might be associated with its higher transmission probability and the absence of anti-resonance transmission around the Fermi energy.

To further reveal the role of destructive QI in the strong conductance suppression of ***m*-CB**, we analyzed the orbital isosurfaces of their HOMO. As shown in Figure 4b, we find the HOMO of the carborane framework shows a peripheral orbital distribution, with a nodal plane between the carborane cage and the phenyl groups (the dashed circle). To form the nodal plane in the HOMO of ***m*-CB** from ***o*-CB**, one of the phenyl groups in ***o*-CB** (such as the semitransparent part of ***o*-CB** in Figure 4b) needs to reverse the signs of its orbital coefficients. As such, from ***m*-CB** to ***p*-CB**, that signs of orbital coefficients of the phenyl group need to reverse again to form

the HOMO of ***p*-CB**. The orbital interactions lead to the HOMO coefficients product of the sulfur atoms in ***o*-CB** and ***p*-CB** show a positive sign, which becomes negative in ***m*-CB** (Supporting Information, Figure S14). According to the orbital symmetry rule, the product of orbital coefficients for the atoms that connecting to electrodes is directly associated with the patterns of QI for π bonds based molecular junctions.[23] Thus, we think that both the π channels from phenyls and the 3c–2e bonding channels from carborane cages contribute to the charge transport through carborane junctions, and the 3c–2e bonding channels in all the three connectivities show destructive QI. Since the destructive QI of π channels also occurs in ***m*-CB**, both the π and 3c–2e bonding channels are suppressed by destructive QI, leading to highly suppressed single-molecule conductance of ***m*-CB**, which is also consistent with the experimental comparison that carborane systems show efficient conductance suppression by destructive QI (Supporting Information, Table S4).

The orbital isosurface also provides the insight to understand the high conductance of ***o*-CB**. As shown in Figure 4b, the two phenyl groups in ***o*-CB** are in close distance, which could introduce intramolecular through-space transmission by the substantial overlap between the two phenyl groups. That overlap vanishes in ***m*-CB** and ***p*-CB**, which is due to the relatively larger distances between the two phenyl groups in their molecular skeletons (Supporting Information, Figure S14). Therefore we can conclude that the high conductance of ***o*-CB** is also contributed by the intramolecular through-space transmission pathway between its two phenyl groups. The intramolecular pathway bypasses the 3c–2e bonding channels of the carborane cages with destructive QI, and the alleviating of destructive QI further boost the charge transport through the ***o*-CB**.[24]

In conclusion, we have demonstrated the presence of QI in charge transport through multicenter bonding system by experimental and theoretical investigation of single-molecule carborane junctions with all possible connectivities. We find that the single-molecule conductance for the three connectivities of carboranes reduces as the following trend: ***o*-CB** > ***p*-CB** > ***m*-CB**, in which the shorter molecule junctions of ***m*-CB** shows lower single-molecule conductance than ***p*-CB**. The DFT calculations also support the length-independent conductance trend, and the orbital symmetry rule provides an intuitive understanding of the QI in carborane system. Owing to the occurrence of destructive QI, the *meta*-connected carborane junctions show strong insulating property within a circa 1.2 nm scale. The understanding of connectivity-dependent charge transport through carboranes provides a guideline to design carborane based molecular electronic devices and a reference to investigate QI in multicenter bonding systems.

Acknowledgements

This work was supported by the National Key R&D Program of China (2017YFA0204902), the Natural Science Foundation of China (Nos, 21722305, 21673195, 21703188, U1705254), China Postdoctoral Science Foundation (No. 2017M622060).

Conflict of interest

The authors declare no conflict of interest.

Keywords: carboranes · conducting materials · electron transport · molecular electronics · single-molecule studies

How to cite: *Angew. Chem. Int. Ed.* **2019**, *58*, 10601 – 10605
Angew. Chem. **2019**, *131*, 10711 – 10715

[1] a) S. Ho Choi, B. Kim, C. D. Frisbie, *Science* **2008**, *320*, 1482 – 1486; b) E. J. Dell, B. Capozzi, J. Xia, L. Venkataraman, L. M. Campos, *Nat. Chem.* **2015**, *7*, 209 – 214; c) J. Liu, X. Zhao, J. Zheng, X. Huang, Y. Tang, F. Wang, R. Li, J. Pi, C. Huang, L. Wang, Y. Yang, J. Shi, B.-W. Mao, Z.-Q. Tian, M. R. Bryce, W. Hong, *Chem* **2019**, *5*, 390 – 401; d) J. Liu, X. Huang, F. Wang, W. Hong, *Acc. Chem. Res.* **2019**, *52*, 151 – 160.

[2] a) D. Z. Manrique, Q. Al-Galiby, W. Hong, C. J. Lambert, *Nano Lett.* **2016**, *16*, 1308 – 1316; b) M. H. Garner, H. Li, Y. Chen, T. A. Su, Z. Shangguan, D. W. Paley, T. Liu, F. Ng, H. Li, S. Xiao, C. Nuckolls, L. Venkataraman, G. C. Solomon, *Nature* **2018**, *558*, 415 – 419.

[3] M. Carlotti, S. Soni, S. Kumar, Y. Ai, E. Sauter, M. Zharnikov, R. C. Chiechi, *Angew. Chem. Int. Ed.* **2018**, *57*, 15681 – 15685; *Angew. Chem.* **2018**, *130*, 15907 – 15911.

[4] a) Y. Li, M. Buerkle, G. Li, A. Rostamian, H. Wang, Z. Wang, D. R. Bowler, T. Miyazaki, L. Xiang, Y. Asai, G. Zhou, N. Tao, *Nat. Mater.* **2019**, *18*, 357 – 363; b) B. Huang, X. Liu, Y. Yuan, Z. W. Hong, J. F. Zheng, L. Q. Pei, Y. Shao, J. F. Li, X. S. Zhou, J. Chen, S. Jin, B. W. Mao, *J. Am. Chem. Soc.* **2018**, *140*, 17685 – 17690; c) J. Bai, A. Daaoub, S. Sangtarash, X. Li, Y. Tang, Q. Zou, H. Sadeghi, S. Liu, X. Huang, Z. Tan, J. Liu, Y. Yang, J. Shi, G. Meszaros, W. Chen, C. Lambert, W. Hong, *Nat. Mater.* **2019**, *18*, 364 – 369.

[5] C. J. Lambert, *Chem. Soc. Rev.* **2015**, *44*, 875 – 888.

[6] a) M. Mayor, H. B. Weber, J. Reichert, M. Elbing, C. von Hänisch, D. Beckmann, M. Fischer, *Angew. Chem. Int. Ed.* **2003**, *42*, 5834 – 5838; *Angew. Chem.* **2003**, *115*, 6014 – 6018; b) C. M. Guédon, H. Valkenier, T. Markussen, K. S. Thygesen, J. C. Hummelen, S. J. Van Der Molen, *Nat. Nanotechnol.* **2012**, *7*, 305 – 309; c) N. Darwish, I. Diez-Perez, P. Da Silva, N. J. Tao, J. J. Gooding, M. N. Paddon-Row, *Angew. Chem. Int. Ed.* **2012**, *51*, 3203 – 3206; *Angew. Chem.* **2012**, *124*, 3257 – 3260; d) R. J. Nichols, S. J. Higgins, *Nat. Nanotechnol.* **2012**, *7*, 281; e) M. Carlotti, A. Kovalchuk, T. Wachter, X. Qiu, M. Zharnikov, R. C. Chiechi, *Nat. Commun.* **2016**, *7*, 13904; f) T. A. Su, M. Neupane, M. L. Steigerwald, L. Venkataraman, C. Nuckolls, *Nat. Rev. Mater.* **2016**, *1*, 16002; g) S. J. van der Molen, R. Naaman, E. Scheer, J. B. Neaton, A. Nitzan, D. Natelson, N. J. Tao, H. van der Zant, M. Mayor, M. Ruben, M. Reed, M. Calame, *Nat. Nanotechnol.* **2013**, *8*, 385 – 389; h) R. J. Nichols, S. J. Higgins, *Annu. Rev. Anal. Chem.* **2015**, *8*, 389 – 417; i) D. Xiang, X. Wang, C. Jia, T. Lee, X. Guo, *Chem. Rev.* **2016**, *116*, 4318 – 4440; j) F. B. Meng, Y. M. Hervault, L. Norel, K. Costuas, C. Van Dyck, V. Geskin, J. Cornil, H. H. Hng, S. Rigaut, X. D. Chen, *Chem. Sci.* **2012**, *3*, 3113 – 3118; k) X. Yin, Y. Zang, L. Zhu, J. Z. Low, Z. F. Liu, J. Cui, J. B. Neaton, L. Venkataraman, L. M. Campos, *Sci. Adv.* **2017**, *3*, eaao2615; l) E. Leary, B. Limburg, A. Alanazy, S. Sangtarash, I. Grace, K. Swada, L. J. Esdaile, M. Noori, M. T. Gonzalez, G. Rubio-Bollinger, H. Sadeghi, A. Hodgson, T. N. Agrai, S. J. Higgins, C. J. Lambert, H. L. Anderson, R. J. Nichols, *J. Am. Chem. Soc.* **2018**, *140*, 12877 – 12883; m) C. R. Arroyo, S. Tarkuc, R. Frisenda, J. S. Seldenthuis, C. H. M. Woerde, R. Eelkema, F. C. Grozema, H. S. J. van der Zant, *Angew. Chem. Int. Ed.* **2013**, *52*, 3152 – 3155; *Angew. Chem.* **2013**, *125*, 3234 –

3237; n) X. Liu, S. Sangtarash, D. Reber, D. Zhang, H. Sadeghi, J. Shi, Z. Y. Xiao, W. Hong, C. J. Lambert, S. X. Liu, *Angew. Chem. Int. Ed.* **2017**, *56*, 173 – 176; *Angew. Chem.* **2017**, *129*, 179 – 182; o) G. C. Solomon, D. Q. Andrews, T. Hansen, R. H. Goldsmith, M. R. Wasielewski, R. P. Van Duyne, M. A. Ratner, *J. Chem. Phys.* **2008**, *129*, 054701; p) S. F. Tan, L. Wu, J. K. Yang, P. Bai, M. Bosman, C. A. Nijhuis, *Science* **2014**, *343*, 1496 – 1499.

[7] L. A. Zotti, E. Leary, M. Soriano, J. C. Cuevas, J. J. Palacios, *J. Am. Chem. Soc.* **2013**, *135*, 2052 – 2055.

[8] a) R. B. King, *Chem. Rev.* **2001**, *101*, 1119 – 1152; b) J. Poater, M. Sola, C. Vinas, F. Teixidor, *Angew. Chem. Int. Ed.* **2014**, *53*, 12191 – 12195; *Angew. Chem.* **2014**, *126*, 12387 – 12391.

[9] a) R. N. Grimes, *Carboranes*, 3rd ed., John Fedor, London, **2016**; b) R. N. Grimes, *Dalton Trans.* **2015**, *44*, 5939 – 5956.

[10] J. Plesek, *Chem. Rev.* **1992**, *92*, 269 – 278.

[11] C. Douvris, C. M. Nagaraja, C.-H. Chen, B. M. Foxman, O. V. Ozerov, *J. Am. Chem. Soc.* **2010**, *132*, 4946 – 4953.

[12] a) G. Vives, J. M. Tour, *Acc. Chem. Res.* **2009**, *42*, 473 – 487; b) M. F. Hawthorne, J. I. Zink, J. M. Skelton, M. J. Bayer, C. Liu, E. Livshits, R. Baer, D. Neuhauser, *Science* **2004**, *303*, 1849 – 1851.

[13] K.-R. Wee, W.-S. Han, D. W. Cho, S. Kwon, C. Pac, S. O. Kang, *Angew. Chem. Int. Ed.* **2012**, *51*, 2677 – 2680; *Angew. Chem.* **2012**, *124*, 2731 – 2734.

[14] A. I. Yanson, G. R. Bollinger, H. E. van den Brom, N. Agrait, J. M. van Ruitenbeek, *Nature* **1998**, *395*, 783 – 785.

[15] a) Y. Quan, Z. Qiu, Z. Xie, *Chem. Eur. J.* **2018**, *24*, 2795 – 2805; b) Y. Quan, Z. Xie, *Chem. Soc. Rev.* **2019**, https://doi.org/10.1039/C9CS00169G.

[16] W. Hong, D. Z. Manrique, P. Moreno-Garcia, M. Gulcur, A. Mishchenko, C. J. Lambert, M. R. Bryce, T. Wandlowski, *J. Am. Chem. Soc.* **2012**, *134*, 2292 – 2304.

[17] CCDC 1900310, 1900311, and 1900312 contain the supplementary crystallographic data for this paper. These data can be obtained free of charge from The Cambridge Crystallographic Data Centre.

[18] T. Hines, I. Diez-Perez, J. Hihath, H. Liu, Z.-S. Wang, J. Zhao, G. Zhou, K. Muellen, N. Tao, *J. Am. Chem. Soc.* **2010**, *132*, 11658 – 11664.

[19] E. Hao, B. Fabre, F. R. Fronczek, M. G. Vicente, *Chem. Commun.* **2007**, 4387 – 4389.

[20] O. Adak, E. Rosenthal, J. Meisner, E. F. Andrade, A. N. Pasupathy, C. Nuckolls, M. S. Hybertsen, L. Venkataraman, *Nano Lett.* **2015**, *15*, 4143 – 4149.

[21] D. Z. Manrique, C. Huang, M. Baghernejad, X. Zhao, O. A. Al-Owaedi, H. Sadeghi, V. Kaliginedi, W. Hong, M. Gulcur, T. Wandlowski, M. R. Bryce, C. J. Lambert, *Nat. Commun.* **2015**, *6*, 6389.

[22] a) M. Brandbyge, J. L. Mozos, P. Ordejon, J. Taylor, K. Stokbro, *Phys. Rev. B* **2002**, *65*, 165401; b) Z. Q. Fan, K. Q. Chen, *Appl. Phys. Lett.* **2010**, *96*, 053509.

[23] a) K. Yoshizawa, T. Tada, A. Staykov, *J. Am. Chem. Soc.* **2008**, *130*, 9406 – 9413; b) C. J. Lambert, S. X. Liu, *Chem. Eur. J.* **2018**, *24*, 4193 – 4201.

[24] L. Chen, Y. H. Wang, B. He, H. Nie, R. Hu, F. Huang, A. Qin, X. S. Zhou, Z. Zhao, B. Z. Tang, *Angew. Chem. Int. Ed.* **2015**, *54*, 4231 – 4235; *Angew. Chem.* **2015**, *127*, 4305 – 4309.

Manuscript received: April 12, 2019
Revised manuscript received: May 26, 2019
Accepted manuscript online: June 5, 2019
Version of record online: June 27, 2019

